



PII S0016-7037(00)00888-2

Solid-state (^1H and ^{13}C) nuclear magnetic resonance spectroscopy of insoluble organic residue in the Murchison meteorite: A self-consistent quantitative analysis

G. D. CODY,^{1,*} C. M. O'D. ALEXANDER,² and F. TERA²¹Geophysical Laboratory and ²Department of Terrestrial Magnetism, Carnegie Institution of Washington, 5251 Broad Branch Road NW, Washington, DC 20015, USA

(Received June 12, 2001; accepted in revised form November 27, 2001)

Abstract—Complementary, double- and single-resonance solid-state (^1H and ^{13}C) nuclear magnetic resonance (NMR) experiments were performed on a solvent extracted and demineralized sample of Murchison meteorite organic macromolecule. These NMR data provide a consistent picture of a complex organic solid composed of a wide range of organic (aromatic and aliphatic) functional groups, including numerous oxygen-containing functional groups. The fraction of aromatic carbon within the Murchison organic residue (constrained by three independent experiments) lies between 0.61 and 0.66. The close similarity in cross-polarized and single-pulse spectra suggests that both methods detect the same distribution of carbon. With the exception of interstellar diamond (readily detected in slow magic angle spinning single-pulse NMR experiments), there is no evidence in the solid-state NMR data for a significant abundance of large laterally condensed aromatic molecules in the Murchison organic insoluble residue. Given the most optimistic estimation, such carbon would not exceed 10% and more likely is a fraction of this maximum estimate. The fraction of aromatic carbon directly bonded to hydrogen is low ($\sim 30\%$), indicating that the aromatic molecules in the Murchison organic residue are highly substituted. The bulk hydrogen content, H/C, derived from NMR data, ranges from a low of 0.53 ± 0.06 and a high of 0.63 ± 0.06 . The hydrogen content (H/C) determined via elemental analysis is 0.53. The range of oxygen-containing organic functionality in the Murchison is substantial. Depending on whether various oxygen-containing organic functional groups exist as free acids and hydroxyls or are linked as esters and ethers results in a wide range in O/C (0.22 to 0.37). The lowest values are more consistent with elemental analyses, requiring that oxygen-containing functional groups in the Murchison macromolecule are highly linked. The combined ^1H and ^{13}C NMR data reveal a high proportion of methine carbon, which requires that carbon chains within the Murchison organic macromolecule are highly branched. Copyright © 2002 Elsevier Science Ltd

1. INTRODUCTION

The organic material in primitive chondritic meteorites has attracted considerable attention, not only because it retains a record of synthesis in the interstellar medium and possibly in the Solar Nebula, but also because it may have been an important component of the prebiotic organic material on the early Earth. Organic material in chondrites can be divided into two fractions (for a review, see Cronin et al., 1988): a soluble fraction composed of a complex mix of compounds, including many amino acids, and an insoluble fraction composed of a largely uncharacterized macromolecular material. The insoluble fraction is thought to be composed of a variety of aromatic ring systems cross-linked by short methylene chains, esters, ethers, sulfides, and biphenyl groups (e.g., Hayatsu et al., 1977; Hayatsu and Anders, 1981; Sephton et al., 2000).

Currently, the origin of the macromolecular material remains an enigma. On the basis of its highly aromatic nature, it was originally suggested that it formed by pyrolytic alteration of aliphatic material produced by Fischer-Tropsch synthesis in the Solar Nebula (Hayatsu et al., 1977; Hayatsu and Anders, 1981). Recent calculations by Kress and Tielens (2001) confirm that Fischer-Tropsch processes could have been relatively efficient in the Solar Nebula. Other mechanisms of synthesis proposed

include: synthesis via electric discharge (Miller, 1955), ultraviolet radiation (Sagan and Khare, 1979), and direct condensation from high temperatures (900 to 1100 K; e.g., Morgan et al., 1991). Note, however, that none of these mechanisms could explain the enormous isotopic fractionations observed in meteoritic organic molecules. It is possible that the macromolecular material formed by thermal alteration of a mixture of more aliphatic interstellar and solar system material in the Solar Nebula (e.g., through lightning, Desch and Cuzzi, 2000, and shock waves, Kress et al., 2001) or perhaps later during the hydrothermal alteration of the meteorite parent body.

There are components within the macromolecular material with large enrichments in deuterium and ^{15}N (Robert and Epstein, 1982; Yang and Epstein, 1983, 1984; Kerridge, 1983, 1985; Kerridge et al., 1987; Alexander et al., 1998), suggesting that at least a proportion of the macromolecule is derived from interstellar material. The isotopic composition of the macromolecular material has been shown to vary from meteorite to meteorite (Kerridge, 1983; Yang and Epstein, 1983; Alexander et al., 1998). Furthermore, the isotopic composition of structurally identical aromatic units also vary from meteorite to meteorite (Sephton et al., 2000). One possible explanation is that variations in the extent of mixing of interstellar medium and solar system material produced a range of compositions in the regions where the chondrites formed. However, the ratio of presolar grains to organics is fairly constant in the most primitive meteorites. A more likely explanation is that variations in

* Author to whom correspondence should be addressed (cody@gl.ciw.edu).

the extent of parent body processing experienced by the meteorites have modified the macromolecular material, as well as its stable isotopic composition (Alexander et al., 1998).

To place some constraint on the various "origin" theories, one has to first establish a chemical structural model of the macromolecule that is consistent with both degradative (extractive) and nondegradative (spectroscopic) analytical schemes. We have chosen to study the macromolecular material in the Murchison (CM2) meteorite because it is a large, well-studied, recent fall (most of the soluble organic studies have concentrated on this meteorite). Also, despite the possibility of some alteration on the parent body (Sephton et al., 2000), its macromolecular material has large D and ^{15}N enrichments, indicative of the survival of some interstellar material. In the work described below, solid-state nuclear magnetic resonance (NMR) spectroscopy is applied to the Murchison organic residue as a complementary and nondestructive method capable of the quantitative determination of the range of organic functionality that constitutes the bulk of the carbon.

To our knowledge, there have only been three published solid-state NMR studies of the organic macromolecule isolated from the Murchison meteorite (two of these studies also included the Orgueil meteorite, and only one included the Allende meteorite). The first study (Cronin et al., 1987) presented solid-state ^{13}C -NMR spectra from extracted and HF/HCl demineralized samples and used standard cross-polarization (CP) and magic angle spinning (MAS) experiments. Their data indicated that the percentage of aromatic carbon constituted ~40% of the total carbon (the amount of aromatic carbon is typically defined as the fraction of aromatic carbon [F_a]; in this case, $F_a \sim 0.40$). CP-MAS NMR may not detect carbon distant from ^1H . Cronin et al. (1987) noted that their value of F_a appeared to be too low given previous estimates of the composition of the Murchison organic matter and single-pulse (SP) ^{13}C solid-state NMR (a method that, in principle, should detect all carbon) and reported that, qualitatively, the aromatic intensity increased, suggesting that there might be carbon that is not detectable via CP methods—for example, carbon in large aromatic domains distant from hydrogen.

More than a decade later, Cody et al. (1999) reinvestigated the insoluble fraction of the Murchison organic assemblage by means of solid-state ^{13}C -NMR. In their study, the extent of demineralization was nearly complete, and the signal to noise was higher than that afforded to Cronin et al. (1987). Cody et al. (1999) concluded from their data that the aromaticity (F_a) was on the order of 0.60. In addition to increased aromaticity, the ^{13}C solid-state NMR spectrum revealed significant quantities of apparently oxygen-containing functional groups, including carbonyls, carboxyls, and either aliphatic ether or alcohols.

Gardinier et al. (2000) published an NMR study of both the Orgueil and the Murchison organic macromolecule. Their results for Murchison indicated an apparent aromaticity (F_a) of 0.52. On the basis of this apparent low aromaticity, Gardinier et al. (2000) shared the conclusion of Cronin et al. (1987) that the CP-MAS NMR experiments must be underestimating nonprotonated aromatic carbon.

Gardinier et al. (2000) reported that their elemental analysis of the Murchison residue yielded a value of H/C equal to 0.72. From their NMR data, however, Gardinier et al. (2000) determined that the bulk hydrogen content (H/C) ranged between

0.84 and 0.93. To accommodate the apparent disparity between the elemental value and that estimated from CP-MAS ^{13}C -NMR, they adjusted their data by adding a contribution of "invisible" (i.e., nondetectable and nonprotonated) aromatic carbon sufficient to raise their F_a values up to a range of 0.61 to 0.68. This correction requires that a substantial percentage of carbon (19 to 33%) is unable to be detected by means of CP-MAS ^{13}C -NMR.

Historically, there is some uncertainty regarding the correct value for H/C. Hayatsu et al. (1977) reported an H/C of 0.76, Robert and Epstein (1982) reported a H/C value of 0.51, Kerridge (1983) reported a H/C value of 0.50, and Gardinier et al. (2000) reported a H/C value of 0.72, whereas determination of the bulk H/C values for the Murchison insoluble organic residue in the present study is 0.53 (see section 2, Experimental, below, for details). It is not immediately obvious which of these measurements is the most accurate. If one considers that the correct H/C value is closer to 0.50 (e.g., Zinner, 1988), then the upper limit in the adjusted F_a derived from the data of Gardinier et al. (2000) could rise as high as 0.79, implying that nearly 60% of the carbon is not detected via CP ^{13}C -NMR.

As it stands, the range in apparent F_a for the Murchison organic macromolecule is enormous, spanning from 0.40 up to nearly 0.80. If NMR data are to be used to constrain a model molecular structure of the insoluble organic fraction from the Murchison meteorite, then the range in probable F_a must be narrowed substantially. The NMR experiments described below seek to do this by establishing an internally consistent set of data, including a narrowly constrained value for F_a , an accurate estimate of the abundance of primary organic functional groups, and robust determination of H/C and O/C. In addition, we seek to explain why the apparent disparity in F_a values exists among the three previously published sets of data.

2. EXPERIMENTAL

2.1. Sample Preparation: Disaggregation and Demineralization

The Murchison sample analyzed in this study was largely covered by fusion crust. This was scraped off with cleaned steel dental tools. The sample was then etched twice in a high-purity mixture of 9 M HF/1 M HCl. Before and after each etch, the sample was ultrasonically cleaned with high-purity water. The sample was then crushed into roughly half-centimeter-size fragments and freeze-thaw-disaggregated in a Teflon container with ultrapure water. After disaggregation, a series of toluene/methanol extractions were conducted to remove as much of the soluble organics as possible.

Our goal for the demineralization was to concentrate the organics without modifying them. We developed a new approach to demineralization that, aside from being less labor-intensive than the conventional HF/HCl method, is both efficient and flexible. As with the conventional HF/HCl technique, the F^- ion was the principal demineralizing agent. In contrast to the conventional HF technique, a fluoride salt (NH_4F , KF, or CsF) was used, thus allowing for the digestion of silicate minerals under a variety of conditions, including at room temperature at pHs of ≤ 9 to 8. A powdered terrestrial rock (e.g., basalt or granite) is fully converted by this technique into HCl-soluble fluorsilicates within hours at room temperature (within minutes at elevated temperatures). In contrast, primitive chondrites are much more resistant, apparently because the minerals are or become encased in carbonaceous material and S° from attacked sulfides.

To overcome this, we capitalized on the relative accessibility of the organic material and their generally hydrophobic nature. We carried out the demineralization reaction in the presence of two immiscible liquids: the aqueous fluoride salt solution and a dioxane- CS_2 mixture. This mixture was mechanically shaken for a minimum of 24 h. After

standing for a few minutes, the emulsified mixture separated into two phases. Dioxane was mutually miscible in H₂O and CS₂, which facilitated the intimate mixing of the immiscible phases during shaking. It also prevented the formation of stable aqueous globules within the CS₂ layer and wet the organics, preventing them from adhering to the walls of the container. The relatively dense unreacted material settled to the bottom of the container; the organic macromolecular material, because of its hydrophobic nature and lower density, concentrated as a thin disk at the interface of the immiscible solutions. The CS₂ acted as a solvent for the elemental S produced when sulfides were attacked.

In the experiments described below, CsF was used because it produces a relatively dense solution of high ionic strength and because Cs⁺ is less likely to interact with the macromolecule than NH₄⁺. A saturated solution of CsF (~30 M) is strongly alkaline, and its density is ~2.7 g/ml. To prepare the salt solution, water and concentrated HF were added until the required pH and density were achieved. Tests on low- and intermediate-rank coals showed that at a pH of 5 to 6, there were no changes in bulk chemistry (detected via NMR spectroscopy). At higher pH, a slight degree of deprotonation of acidic phenolic groups (~2 to 3%, determined by solid-state ¹³C-NMR) was observed.

The sample, salt solution, and dioxane-CS₂ mixture (40 to 50% CS₂) were combined in tightly capped Teflon tubes and shaken. Liberation of the organics began within hours. Because of the density of the salt solution, upon standing, the organics floated up to the interface of the immiscible liquids, and the more dense material sank to the bottom. The liberated organics were extracted after centrifugation, then washed in a ~1:1:1 mixture of dioxane-CS₂-water. HCl (HCl ~1 M) was added to remove CsF, elemental S, and any other soluble material. The final dried residue had an ash weight of ~9 wt%.

2.2. Elemental Analysis

Elemental analysis (H, C, and N) was performed on 0.78 mg of dry sample yielding 51.2 wt% C, 2.25 wt% H, and 1.74 wt% N, corresponding to a formula of C₁₀₀H_{52.7}N_{2.9}. Direct determination of oxygen content via combustion/mass spectrometry was performed on 0.513- and 1.17-mg samples and yielded an average value of 16.8 ± 0.1 wt% O, yielding 25 O/100 C. The ash weight was 9.3 wt%, leaving a difference of 18.7 wt%, which is attributed to sulfur. The majority of this sulfur is S⁰ produced during the demineralization of sulfides.

2.3. Solid-State NMR Spectroscopy

All experiments described in this report were performed with a Varian-Chemagnetics Infinity solid-state NMR spectrometer. The static field strength of the magnet is ~7.05 T, and the Larmor frequencies of ¹H and ¹³C at this field strength are ~300 and 75 MHz, respectively. All ¹³C-NMR experiments were performed with a 5-mm double resonance MAS probe. The spectra were referenced to hexamethyl benzene (a secondary reference) and are presented as frequencies in part-per-million shift relative to that of the methyl group in tetramethylsilane.

All CP experiments used a ¹H 90° pulse width of 4 μs; the delay between acquisitions was 1 s, the spectral width was 50 kHz, and the acquisition time was 2.56 ms. Both the ¹H spin-lock and decoupling B₁ frequencies were fixed at 62.5 kHz. CP experiments performed at relatively slow spinning rates (4 kHz) used a standard (static value) Hartmann-Hahn match (Hartmann and Hahn, 1962). Variable contact time experiments were used to determine the optimum contact time (see details below).

High-speed (MAS frequencies of 12 kHz) CP experiments require the use of the variable-amplitude CP (VACP) method where, during the contact time, the strength of the carbon B₁ field was stepped over a range of magnitudes below that of the static match frequency. Both high- and low-speed MAS CP experiments were optimized to yield the correct functional group distributions for a variety of organic standards, including the following: dimethyl naphthalene, chrysene, syringic acid (3,5 dimethoxy-4-hydroxy benzoic acid), syringaldehyde (4-hydroxy-3,5-dimethoxybenzaldehyde), and hexamethylbenzene. The CP spectra are the sum of 312,000 acquisitions coadded and Fourier-transformed together.

Solid-state ¹³C SP (Bloch decay) MAS experiments were run to compare and contrast the effects of deriving carbon signal from proximal hydrogen (e.g., CP) with spectra in which all ¹³C nuclei are

excited, regardless of proximity to hydrogen (e.g., SP). The spectral widths, acquisition times, and ¹H decoupling fields were identical to those used in the CP experiments. In general, after a 90° rotation ¹³C pulse, it is necessary to wait up to five times T₁ (where T₁ is the spin-lattice relaxation time) between acquisitions to avoid signal saturation. Typical values of T₁ for coals are on the order of 20 to 30 s (e.g., Tsiao and Botto, 1993); thus, an acquisition delay of 100 s is sufficient. The relatively low value of T₁ for coals is largely attributable to the presence of unpaired electrons (on the order of 10¹⁸ to 10¹⁹ per gram of carbon; see van Krevelan, 1993). Electron paramagnetic measurements of the Murchison organic fraction record a value of 1.5 × 10¹⁸ unpaired electrons per gram of carbon (Cronin et al., 1987).

In our experiments, a ¹³C pulse width of 1.3 μs, corresponding to a 30° rotation angle, was used. The small rotation angle allows for a shorter delay between acquisitions and minimizes the potential for longitudinal interference due to incomplete relaxation of the ¹³C nuclei (e.g., Ernst et al., 1991). Thus, an acquisition delay of 10 s was used, ensuring that all carbon with T₁ values of less than 50 s would not suffer any signal loss due to longitudinal interference. A total of 24,000 acquisitions were added and Fourier-transformed to yield the final spectra.

Solid-state ¹H-NMR spectra were acquired with a high-speed MAS probe that used 2.5-mm zirconia sample rotors. MAS frequencies of 30 kHz (the maximum safe speed for this probe) were used. The ¹H background signal from the probe was suppressed with a standard 16-pulse cycle sequence. The specific acquisition parameters included a 2.5-μs 90° proton pulse width, a spectral width of 200 kHz, a recycle delay of 2 s, and an acquisition time of 5 ms. A total of 6400 acquisitions were added and Fourier-transformed to yield the final spectrum.

3. RESULTS AND DISCUSSION

3.1. NMR Spectroscopy

Thorough descriptions of NMR spectroscopy can be found in numerous texts. In the interest in ensuring accessibility to readers unfamiliar with NMR, we provide a brief general description. The heart of a NMR spectrometer is a high static field magnet. The sample is placed at the center of the field, where the spins of nuclei align with and precess around the static field at their characteristic (Larmor) frequencies. Not all isotopes have the nuclear property of spin; for example, ¹²C has no spin, whereas ¹³C is a spin 1/2 particle.

Signal is measured after spins in the sample have resonantly absorbed radio frequency (RF) irradiation and exist in an excited state. The excited spin particles emit an RF signal that, when transformed into the frequency domain, produces a spectrum characteristic of the chemistry of the system. The analytical basis of NMR spectroscopy is derived from the small perturbation in the Larmor frequency of a "bare" nucleus (e.g., ¹H or ¹³C) by the electron current density associated with the inner and outer shell electrons surrounding the nucleus—that is, the bonding environment influences the NMR spectrum. As a result of this perturbation, the resonant frequencies of RF excited nuclei in different electronic environments are separated into a spectrum. The magnitude of this perturbation is small, so that the NMR spectra record the position of resonances relative to a standard reference frequency. The position of the resonant frequencies in a NMR spectrum may be assigned to specific functional groups. One of the advantages of NMR spectroscopy is that the probability of transition between spin states, and hence intrinsic resonance intensity, is the same for any given nucleus in any electronic environment.

High-resolution spectroscopy in the solid state is generally only possible through the application of magic angle sample

spinning. In this case, the sample is physically rotated rapidly (in the thousands of hertz) at an angle of 54.7° relative to the static field. The rapid spinning at this angle averages out many of the interactions that lead to severe line broadening inherent in solids. Spinning at frequencies that are less than the strength of a given line broadening interaction (e.g., dipolar coupling between nuclei) leads to a redistribution of signal intensity away from a specific resonance peak into a manifold of peaks appearing at integral values of the rotation frequency. These additional peaks are referred to as spinning side bands and their intensities must be taken in to account when calculating the relative abundance of functional groups.

3.2. CP Variable Contact Time Experiments

The essence of the CP experiment is that ^{13}C acquires its magnetization through "contact" with a fully polarized ^1H spin system. Contact is made by using the ingenious approach described by Hartmann and Hahn (1962), wherein nuclei with different resonant frequencies (at a given static magnetic field) can be brought into contact (coupled) when directed via RF irradiation into a doubly rotating reference frame. By careful adjustment of the ^1H and ^{13}C RF fields, the difference in precession frequencies of both nuclei in the tipped rotating reference frame can be made to vanish. At this point, magnetization from one nuclear spin system can transfer to the other.

The CP method has been shown to be particularly useful in the case where one has an abundant spin reservoir (e.g., ^1H) and a dilute spin reservoir (e.g., ^{13}C) (Pines et al., 1973). This stated, the coupling of the two spin systems is temporary and the magnetization transfer is time dependent; thus, CP methods suffer from relatively complex dynamic effects that can lead to inaccurate conclusions regarding chemical structure (see, e.g., Wind et al., 1993).

The time dependence of magnetization (hence signal intensity) for the targeted nuclei (^{13}C in our case) is given by Eqn. 1 (Mehring, 1976):

$$M_c(\tau) = 4M_0(1 - T_{\text{CH}}/T_{1\rho})^{-1} [\exp(-\tau_{\text{CT}}/T_{1\rho}) - \exp(-\tau_{\text{CT}}/T_{\text{CH}})] \quad (1)$$

where T_{CH} is the time constant governing the rate of magnetization transfer, $T_{1\rho}$ is the spin-lattice relaxation time in the rotating frame (the quantity that places the limit on the time two nuclear spin systems can remain coupled in the rotating reference frame), τ_{CT} is the time during which the two spin systems are actually coupled in the rotating frame (i.e., contact time of the experiment), and M_0 is the thermal equilibrium value of ^{13}C magnetization at the given static field.

Ideally for CP, the spin lattice relaxation in the rotating frame should be slow and the magnetization transfer be rapid—that is, $T_{\text{CH}} \ll T_{1\rho}$. However, in practice, this is not often the case. The rate of magnetization transfer is proportional to the magnitude of the strength of dipolar coupling between ^1H and ^{13}C ; consequently, ^{13}C nuclei surrounded by ^1H (e.g., CH_2 groups) will gain magnetization quickly, whereas ^{13}C nuclei one or more bonds away from a ^1H will gain magnetization more slowly. Although CH_3 groups have an abundance of ^1H , they tend to rapidly rotate, thus reducing the strength of the dipolar coupling between ^1H and ^{13}C and reducing the rate of magnetization transfer.

The sum of these dynamic effects are illustrated in Figure 1. By measuring the signal intensity of aliphatic carbon at a chemical shift of 33 ppm (CH_2 , CH , or both) and the signal intensity of aromatic carbon at 129 ppm over a range of contact times, one can follow the buildup and decay of magnetization due to T_{CH} and $T_{1\rho}$. The data in Figure 1A are from a the relatively slow spinning (4 kHz) experiment, where it is clear that the growth in magnetization of aliphatic carbon (33 ppm) is much faster than aromatic carbon (129 ppm); the aliphatic carbon magnetization peaks at a contact time of ~ 1 ms, whereas the aromatic intensity continues to grow reaching its peak at a contact time of ~ 2 ms. The magnetization of both types of carbon decays beyond a contact time of 3 ms.

These data reveal that provided one is willing to lose signal intensity ($\sim 50\%$), a choice of a contact time near 3 ms will yield a largely representative spectrum reflecting the correct relative proportions of aromatic and aliphatic carbon. However, if a contact time between 1 to 2 ms is chosen, then the contribution to the spectrum from aliphatic carbon will be grossly overrepresented. In the study by Cronin et al. (1987), a contact time of 1 ms was chosen, suggesting that their observed low relative abundance of aromatic carbon resulted from an overcontribution from aliphatic carbon due to incomplete magnetization transfer to aromatic carbon.

At higher spinning speeds (e.g., 12 kHz) and with the application of the VACP method for polarization transfer, the situation remains qualitatively the same (Fig. 1B). The application of VACP generally increases the effective T_{CH} , also the strength of the dipolar coupling decreases with increased sample spinning speed, resulting in a further reduction in the magnetization transfer rate. As a result, whereas at 4 kHz sample spinning a contact time of greater than 2 ms is required to obtain representative spectra, at 12 kHz (and with VACP) contact times greater than 3 ms are required to ensure that spectra are obtained with representative distributions of functional groups.

The data in Figure 1B suggest why the observed aromaticities for the Murchison meteorite reported by Gardinier et al. (2000) were so low. Their analyses used a 9.4-T static field NMR system, requiring 15 kHz sample spinning to minimize interference due to spinning side bands, as well as VACP to enhance polarization transfer. However, Gardinier et al. (2000) chose a 1-ms contact time for their experiments. From the data in Figure 1B, it is clear that the combination of fast sample spinning and VACP requires a contact time of at least 3 ms to record spectra with a representative abundance of organic functional groups. With a contact time of only 1 ms, there will be an overrepresentation of the aliphatic carbon as a result of incomplete magnetization transfer to aromatic carbon, yielding an artificially low estimate of aromaticity.

In consideration of the data presented in Figure 1, all the CP experiments discussed below use a contact time of 3 ms for slow spinning (4 kHz) experiments and 4 ms for fast spinning (12 kHz) VACP experiments.

3.3. Variable Amplitude CP and 12-kHz MAS Analysis of the Murchison Organic Matter

The VACP (12 kHz) MAS spectrum of the Murchison organic residue is presented in Figure 2. Although the spectrum

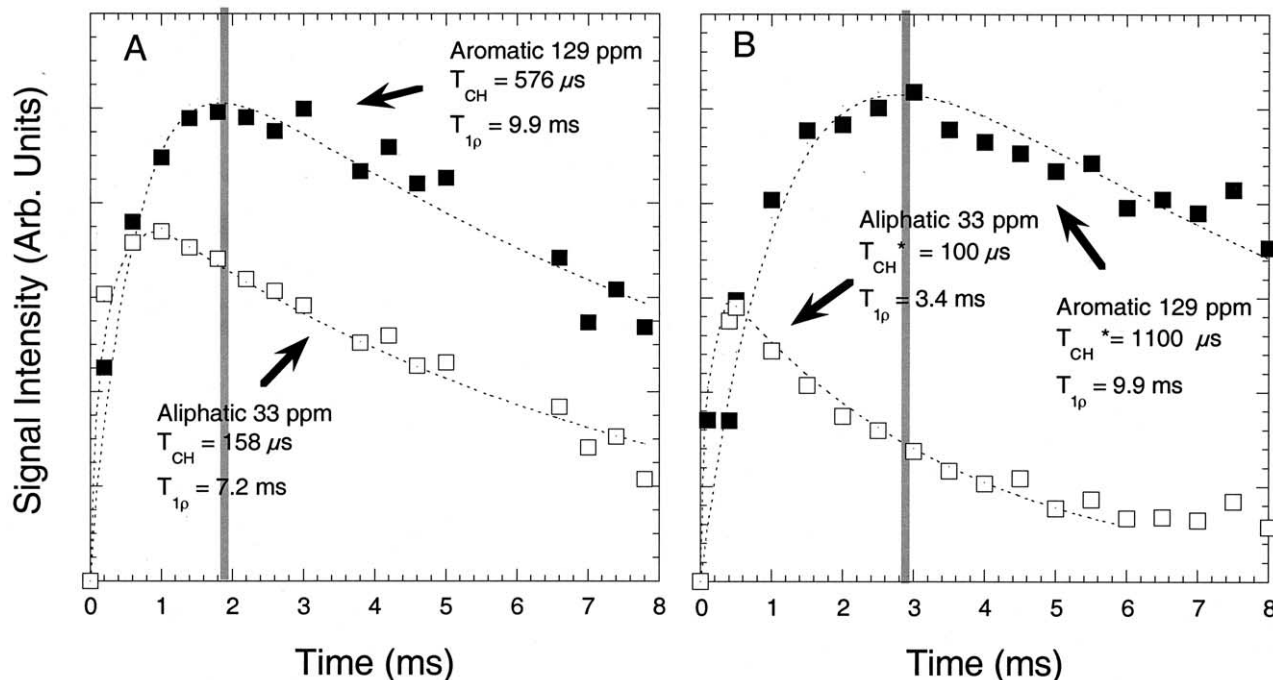


Fig. 1. Variable contact time experiments for ^1H - ^{13}C CP solid-state NMR. Solid squares = intensity of aromatic carbon (129 ppm); open squares = intensity of aliphatic carbon (33 ppm). (A) Change in intensity with contact time with slow MAS (4 kHz). Magnetization transfer is much faster for aliphatic carbon. Full magnetization transfer is achieved at a contact time of ~ 2 ms. The decay in magnetization at times greater than 2 ms is caused by spin lattice relaxation in the rotating frame and is governed by $T_{1\rho}$. (B) Relatively fast MAS (12 kHz) combined with VACP results in a reduction in the rate of magnetization transfer to aromatic carbon such that only after 3 ms, is there a representative amount of magnetization distributed across aromatic and aliphatic carbon.

exhibits considerable inhomogeneous broadening, there are distinct peaks highlighting the contributions of specific organic functional groups. Moving down field (up in frequency and chemical shift ppm), a peak attributed to methyl (CH_3) groups is observed with a chemical shift of ~ 16 ppm. There exists a broad range of frequencies that may be attributable to methyl groups, the width of this range being a function of both intramolecular (i.e., substituent effects such as aliphatic vs. aromatic) and intermolecular (i.e., shielding effects due to proximity with the face of aromatic rings) (Werhli and Wirthin, 1976). The position of the methyl resonance at ~ 16 ppm is low for a methyl group bonded directly to an aromatic molecule, but is consistent with a $\beta\text{-CH}_3$ in an ethyl group on an aromatic ring (e.g., Snape et al., 1979).

The broad peak at ~ 33 ppm likely indicates the presence of both methylene (CH_2) and methine (CH) groups, the later more likely contributing to the down field region of the peak (i.e., 40 to 50 ppm). The pronounced peak at ~ 64 ppm is assigned to oxygen-substituted sp_2 carbon—for example, $\text{CH}_n\text{OH}_{i=0,1}$, where n can range from 0 to 2 (the characteristic frequency of methoxy groups (CH_3O) is too low to be considered) depending on whether the oxygen-substituted carbon is tertiary, secondary, or primary and depending on whether the functional group is an alcohol or an ether, $i = 0$ or 1 (Werhli and Wirthin, 1976).

The most prominent peak in the Figure 2 is at ~ 129 ppm and is assigned to aromatic carbon. The width of this peak is broad, indicating that aromatic carbon in the Murchison organic res-

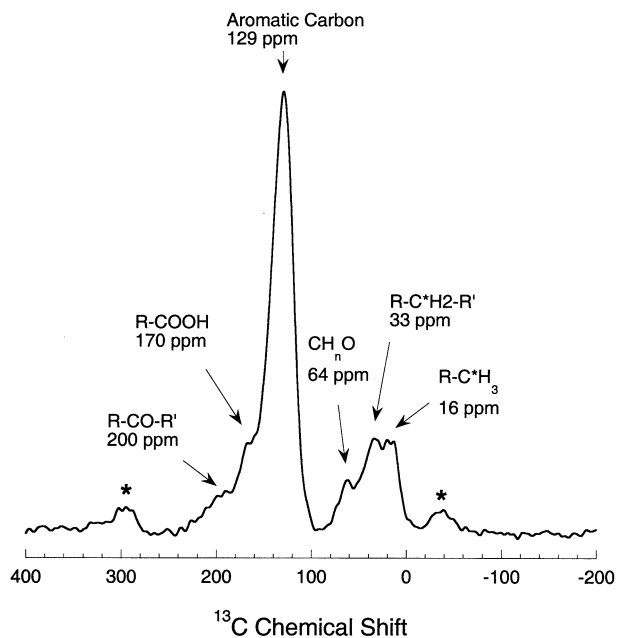


Fig. 2. VACP spectrum (12-kHz MAS) of the Murchison organic macromolecule. Prominent peaks and shoulders are assigned to probable functional groups identified by their respective chemical shifts in ppm, the shift in frequency relative to the carrier frequency, ~ 75 MHz, referenced to tetramethylsilane (TMS). The spinning side bands are designated by an asterisk.

Table 1. Functional group assignment for Murchison macromolecule derived from cross-polarization (VACP) solid-state NMR (MAS frequency, 12 kHz).

Carbon type	Shift (δ) (ppm)	% of total	$C_{100}H_n$	$C_{100}O_m$
CH ₃	15	8.0	24	0
CH, CH ₂	32	8.7	8.7–17.4	0
CH _{n = 1-2} OH _{i = 0,1}	63	5.5	0.0–16.5	5.5 (max)
Aromatic (C-H, C-R)	122	21.5 ^a	0–21.5	0
Aromatic (C-H, C-R)	133	21.5 ^a	0–21.5	0
Aromatic (C-H, C-R)	143	10.7 ^a	0–10.7	0
Aromatic (C-O)	150	7.6 ^a	0–7.6	7.6 (max)
R-COOH,R'	168	7.4 ^a	0–7.4	14.8 (max)
R-CO-R'	195	9.1 ^a	0	9.1
		$F_a = 0.61$	$n = 32.7 - 126.6$	$m = 26.8 - 37.0^b$ O/Ring = 0.74

^a Includes intensity of the corresponding ± 1 spinning side bands.

^b The minimum value corresponds to all COOR groups being linked as aromatic esters, the remaining phenyl-O linked as alkyl aromatic ethers, and the remaining aliphatic-O being in the form of aliphatic ethers. The maximum corresponds to all free acids (COOH and phenyl-OH) and the aliphatic-O groups being entirely alcohol.

idue exists in many different local electronic environments. In general, the region spanning ~ 100 to 129 ppm can be attributed to protonated aromatic carbon. The region from ~ 129 to ~ 150 ppm can be attributed to nonprotonated aromatic carbon, whereas the region from ~ 145 to ~ 160 ppm can be attributed to oxygen-substituted aromatic carbon. However, these designations constitute approximate values. Given that the aromatic region is virtually devoid of any fine structure, any quantitative assessment that is based on a fit of the aromatic region must be considered suspect.

The clearly defined shoulder at ~ 170 ppm corresponds to the presence of carboxylate (COOR), where the COOR might be an ester or an acid. At a chemical shift near 170 ppm, nitrogen bearing functional groups such as amide (CONH) and amidines (CNNH) might also contribute intensity. At ~ 200 ppm, there is another clearly defined shoulder assigned to carbonyl (C=O), where the carbonyl may be either a ketone or aldehyde. Finally, there are the prominent spinning side band peaks associated with aromatic carbon centered at 289 and -31 ppm (± 12 kHz from the center of the aromatic peak at 129 ppm).

3.4. Functional Group Analysis Derived from VACP Spectral Data

The spectrum in Figure 2 was fitted with gaussian peaks to obtain an assessment of the aromaticity (F_a), as well as NMR derived bulk parameters, such as hydrogen and oxygen content. The results are presented in Table 1. The aliphatic region was fitted with three gaussian peaks at 15 , 32 , and 63 ppm. The aromatic region was fit with four gaussian peaks centered at 122 , 133 , 143 , and 150 ppm. The aromatic region could be fit equally well with two gaussian peaks, as was done by Gardinier et al. (2000); however, given that it is well established that oxygen-substituted aromatics are present in the Murchison organic residue (e.g., Hayatsu et al., 1977; Hayatsu and Anders, 1980; Sephton et al., 2000), a peak centered at 150 ppm is included to account for oxygen bearing aromatics. Both the COOR and CO regions were fitted with single gaussian peaks at 168 and 195 ppm, respectively.

Carbon aromaticity, F_a , is 0.61 , a value essentially identical to the previously reported value of 0.60 by Cody et al. (1999),

which was based on a different sample of the Murchison organic residue and derived from a VACP MAS spectrum by using a different set of optimized acquisition parameters with a higher MAS speed (15 kHz). The range in hydrogen content, n (i.e., $C_{100}H_n$), is derived by considering the contribution of hydrogen from each functional group. The uncertainty regarding the identity of specific functional groups—for example, protonated and nonprotonated aromatic carbon—results in a range of n from 32.7 to 126.6 (Table 1). The lower limit considers all aromatic carbon to be nonprotonated, the oxygen-substituted carbon to be a tertiary ether, the carboxylate to be an ester, and the carbonyl to be a ketone. The upper limit is derived by assuming that all the aromatic carbon is protonated, the oxygen-substituted carbon is a primary alcohol, and the carboxylate is an acid.

Determination of the number of oxygens (m) per 100 carbons reveals a range from 26.8 to 37.0 . The maximum is derived by assuming that all oxygen-substituted alkyl carbon is in the form of alcohol, all the oxygen-substituted aromatic carbon is hydroxyl, and the carboxylate is in the form of free acid. The minimum value of m is derived by assuming that all carboxylate is linked to aromatic carbon via aromatic esters, the remainder of aromatic oxygen is linked to aliphatic carbon via alkyl aryl ethers (see, e.g., Hayatsu et al., 1980), and that the remainder of the aliphatic oxygen linked as aliphatic ethers. The direct measurement of the oxygen content of the residue in this study indicates a value of $m = 25$. Hayatsu et al. (1980) reported $m = 12.2$ determined by difference.

The minimum value of m in Table 1 is closest to the direct determination of $m = 25$. A similar analysis of the spectral data reported by Gardinier et al. (2000) yields a range in m from 22.7 to 37.0 . However, in the spectral fit of their data on the Murchison organic residue, the potential contribution of oxygen-substituted aromatic carbon was not considered. If a range for m is calculated from the data in Table 1 assuming that there is no oxygen-substituted aromatic carbon, then the range of m drops to 23 to 29.4 . Where, the minimum now corresponds to all of the oxygen-substituted carbon linked to carboxyl in the form of aliphatic esters, and remaining carboxyl being free acid.

Table 2. Functional group assignment for Murchison macromolecule derived from single pulse (SP)-solid state NMR (MAS frequency = 12 kHz).

Carbon type	Shift (δ) (ppm)	% of Total	$C_{100}H_n$	$C_{100}O_m$
CH_3^a	15	9.7	29.1	0
CH, CH_2^a	32	5.8	5.8–11.6	0
$CH_{n=1-2}OH_i = 0,1$	63	3.1	3.1–9.3	3.1 (max)
Aromatic (C-H, C-R)	122	20.4 ^a	0–20.4	0
Aromatic (C-H, C-R)	133	19.0 ^a	0–19.0	0
Aromatic (C-H, C-R)	143	13.6 ^a	0–13.6	0
Aromatic (C-O)	150	9.6 ^a	0–9.6	9.6 (max)
R-COOH,R	168	6.8 ^a	0–6.8	13.6 (max)
R-CO-R'	195	12.0 ^a	0	12.0 (max)
			$n = 38.0 - 119.4$	$m = 28.6 - 38.3$
		$F_a = 0.63$		O/Ring = 0.9

^a Includes intensity of the corresponding ± 1 spinning side bands.

^b The minimum value corresponds to the case where all COOR groups are linked to form aromatic esters, the remaining phenyl-O linked as alkyl aromatic ethers, and the remaining aliphatic-O being in the form of aliphatic ethers. The maximum corresponds to all free acids (COOH and phenyl-OH) and the aliphatic-O groups being entirely alcohol.

If we assume that the lowest NMR derived values for oxygen content are more likely to be correct, by virtue of being closest to the elemental analysis, then it is required that there exists a maximum degree of linking among oxygen bearing functionality. Specifically, esters as opposed to free acids, and ethers as opposed to free hydroxyls (either aliphatic or aromatic). It is further noted that the estimates of hydrogen content are linked to that of oxygen content; thus, the lower oxygen contents correlate with the lower hydrogen contents (Tables 1 and 2).

3.5. SP ^{13}C MAS (12 kHz) NMR of the Murchison Organic Residue

It is well known that in the case of thermally mature coals, where the hydrogen contents are low, NMR spectra obtained via CP can underestimate the contribution of carbon distant from hydrogen, for instance if there were substantial quantities of large laterally condensed aromatic molecules present such as coronene, ovalene, and larger. SP ^{13}C -NMR is not subject to such a bias because it detects carbon directly rather than relying on magnetization transfer from the 1H spin reservoir. In Figure 3, the SP ^{13}C -NMR spectrum of the Murchison organic residue is presented. In comparison with the CP ^{13}C -NMR spectrum (Fig. 2), it is immediately apparent that the signal to noise is considerably less. This is an accepted drawback when SP NMR is used because it is an intrinsically less sensitive technique (Pines et al., 1973).

Aside from the reduction in signal to noise, the SP ^{13}C -NMR spectrum (Fig. 3) of the Murchison organic residue is not strikingly different than the CP ^{13}C -NMR spectrum (Fig. 2). Slight differences in functional group representation derived from SP vs. CP NMR are apparent in the low-frequency region of the spectrum where there is a reduction in the relative amount of methylene, methine, and oxygen-substituted aliphatic carbon. In the high frequency region, there is a slight increase in the relative abundance of carbonyl. Overall, however, the aromaticity (F_a) increases only slightly to 0.63 (Table 2). The NMR-derived values of hydrogen content, using the identical scheme used above for the CP ^{13}C -NMR data, reveal a range from 34.9 to 119.4 hydrogens/100 carbons (Table 2). The NMR derived values for oxygen content reveals a range from 28.6 to 38.3 oxygens/100 carbons (Table 2). If we again

assume that there is essentially no oxygen-substituted aromatic carbon, the range in oxygen content shifts down to a low of 25.6 and a high of 28.7.

The similarity of the SP and CP spectra (Figs. 2 and 3) and data derived from them (Tables 1 and 2) does not support the hypothesis that there is a substantial reservoir of hydrogen poor carbon that is "invisible" to CP NMR methods. Rather, these data suggest that in the case of the Murchison organic residue, the CP and SP experiments detect the same range of carbon functionality and in similar abundance.

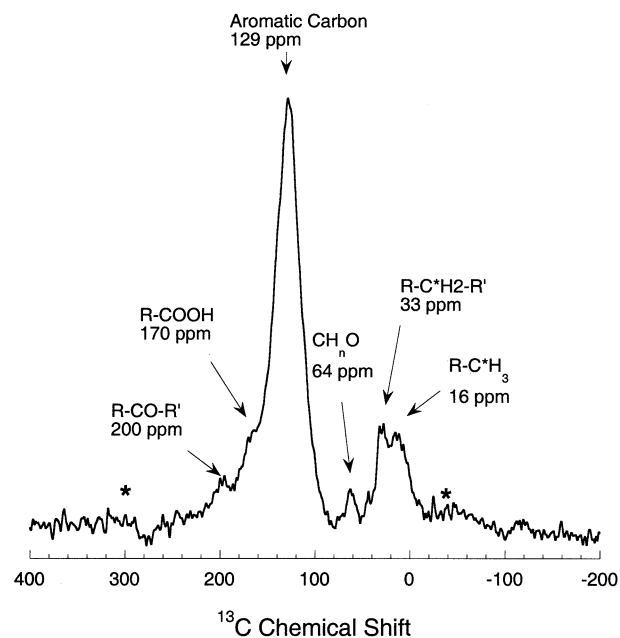


Fig. 3. SP spectrum (12-kHz MAS) of the Murchison organic macromolecule. Prominent peaks and shoulders are assigned to probable functional groups identified by their respective chemical shifts in ppm, the shift in frequency relative to the carrier frequency, ~ 75 MHz, referenced to tetramethylsilane (TMS). The spinning side bands are designated by an asterisk.

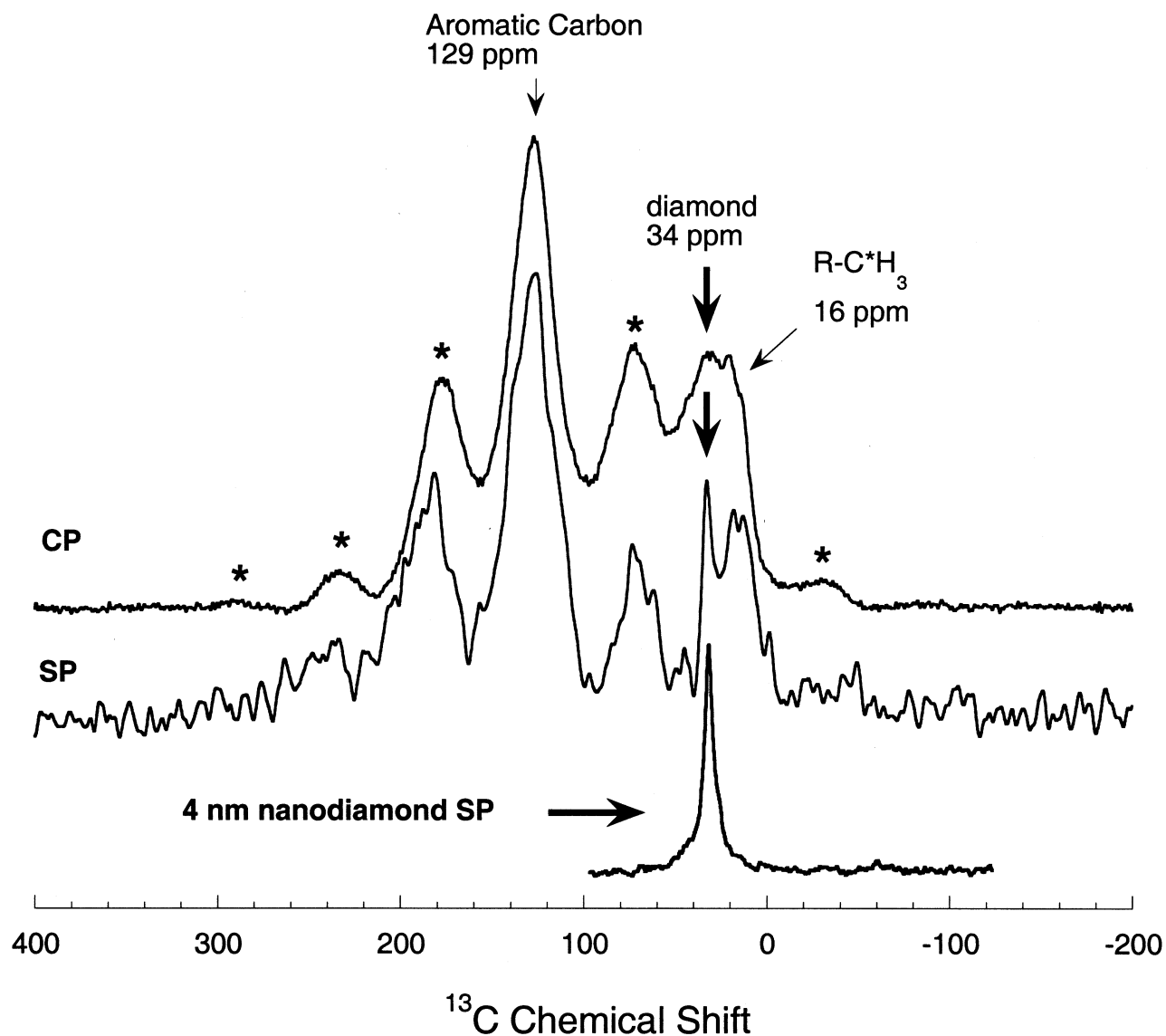


Fig. 4. Slow MAS (4 kHz) NMR spectra. Presented are a standard CP spectrum and a SP spectrum of the Murchison organic macromolecule. The intense aromatic spinning side bands are labeled with asterisks. The sharp peak present in the middle SP spectrum is assigned to the diamond resonance (34 ppm). For reference, an SP spectrum of 4 nm (detonation) diamond powder is presented at the bottom (single peak at 34 ppm). No signal is observed for carbon in diamond via CP methods.

3.6. Slow MAS Experiments: CP and SP on the Murchison Organic Residue

Additional and independent chemical structural information can be obtained with experiments run at lower spinning speeds (4 kHz in this case) by exploiting the effects of increased dipolar coupling between ^1H and ^{13}C . The disadvantage of slow sample spinning is that carbon in bonding environments with large degrees of chemical shielding anisotropy (e.g., aromatic carbon) will lose a significant proportion of their spectral intensity into a large manifold of spinning side bands. These side bands arise at \pm integral values of the rotor speed (at 4 kHz these are at $\pm n \times 53$ ppm). Particularly problematic is the case of the intense aromatic peak at 129 ppm (Figs. 2 and 3), where the high field spinning side bands occur at 76 and 22

ppm, leading to substantial overlap with aliphatic carbon. An unanticipated positive attribute in the case of the Murchison organic residue is that small quantities of carbon in high symmetry environments (where the chemical shielding anisotropy is low) will have their sensitivity proportionately enhanced because they do not produce significant side bands.

In Figure 4, slow CP and SP MAS spectra of the Murchison organic residue are presented. At a glance, one may observe that the slow 4-kHz spectra differ enormously from the 12-kHz spectra, principally because of the significant intensity of the spinning side bands derived from the intense aromatic peak centered at 129 ppm. As was the case with the 12-kHz spectra (Figs. 2 and 3), the SP spectrum of the Murchison in Figure 4 also exhibits much lower signal to noise relative to the CP experiment.

The most striking difference between the CP and SP spectra is the presence of a sharp peak in the SP spectrum at 34 ppm. This peak is coincident with the single carbon resonance observed in diamond. At the base of Figure 4, an SP ^{13}C spectrum of 4-nm detonation diamonds is included demonstrating the coincidence in resonance frequency at 34 ppm. Spectra of larger diamond particles (up to 250 nm; data not shown) also exhibit a single sharp resonance at 34 ppm.

The existence of nanodiamonds within the Murchison meteorite, as well as in other carbonaceous chondrites, is well known (e.g., Lewis et al., 1987). In the Murchison meteorite, nanodiamonds have been reported to be present at concentrations of ~ 400 ppm ($\sim 3\%$ of the macromolecular carbon in the case of the Murchison insoluble residue) (Lewis et al., 1987). Integration of the SP spectrum in Figure 4 reveals that the proportion of the sharp 34 ppm signal to the total signal intensity is $2.9 \pm 0.2\%$ (where the error accounts for an uncertainty in the fit on the order of $\pm 10\%$). The straightforward detection of diamond in the Murchison insoluble organic residue likely results from the presence of extensive defects and associated paramagnetic centers within them.

The significance of the detection of interstellar diamonds via slow spinning SP ^{13}C -NMR is twofold. First, the detection of interstellar diamond highlights the fact that large carbonaceous domains distant from hydrogen are readily detected when present with SP NMR. This means that if there were significant domains of nonprotonated aromatic carbon these too should be detected. Second, the relative concentration of interstellar diamond is close to that reported via degradative methods (e.g., Lewis et al., 1987), indicating that the SP NMR spectra (Figs. 3 and 4) report a representative picture of the distribution of organic carbon in Murchison. Given the discussions above regarding the similarity between the VACP and SP with relatively fast MAS, it then appears reasonable to infer that CP methods also yield a representative picture of the functional group chemistry in the Murchison insoluble organic fraction.

Finally, it is interesting to consider why interstellar diamond is detected so readily in the 4-kHz SP spectrum and is not as apparent in the 12-kHz SP spectrum (Fig. 3). Careful inspection of Figure 3 reveals a sharpening of the 33-ppm peak (labeled in Fig. 3 as "methylene") consistent with the presence of interstellar diamond. As stated above, with slower sample spinning, resonance intensity of carbon in less symmetric environments diminishes as intensity is redistributed into the multiple spinning side bands. In the case of diamond, the extremely high symmetry of the electronic environment surrounding the carbon nucleus results in minimal side band intensity relative to that of methine or methylene carbon. Therefore, with slower sample spinning, although all other peaks shrink in intensity, the diamond resonance will remain essentially unchanged, and hence, it appears more pronounced. If the data presented in Table 1 are corrected for the $\sim 3\%$ interstellar diamond, the SP value for F_a will increase to 0.65.

3.7. Interrupted Decoupling Experiments Using CP and Slow Sample Spinning

The conclusion that CP experiments provide a representative picture of the distribution of organic functional groups in the Murchison insoluble organic fraction creates the opportunity of

applying two powerful experiments that can provide complementary data to support the aforementioned discussions. First, in the discussions of the aromatic carbon peaks detected via high-speed MAS using both the VACP and SP methods (Tables 1 and 2), it was acknowledged that it was not possible to assess the extent to which aromatic carbon is protonated; a designation by peak position is not satisfactory. This uncertainty in spectral assignment leads to the large uncertainties in the NMR-derived hydrogen content (see Tables 1 and 2).

Interrupted decoupling experiments provide a means of determining the fraction of protonated to nonprotonated aromatic carbon (e.g., Alemany et al., 1983). This experiment is a variation of the standard CP experiment wherein a delay period (variable in length) is inserted immediately after the contact pulse and before the acquisition time. During this delay, high power ^1H decoupling is gated off allowing dipolar coupling between ^1H - ^{13}C spins to induce a loss in phase coherence of the ^{13}C magnetization, leading to a loss in signal intensity.

The rate of decay in signal intensity due to dipolar dephasing is proportional to the distance between ^{13}C and ^1H , as well as the number of hydrogen nearest neighbors. The dynamics of signal loss exhibits the following useful property: carbon that is directly bonded to a hydrogen exhibits a Gaussian decay—that is, where $I = I_0 \exp(-T_{\text{dd}}^2/2T_{2a}^2)$ —and carbon not directly bonded to hydrogen exhibits a Lorentzian decay—that is, where $I = I_0 \exp(-T_{\text{dd}}/T_{2b})$. The exception to this is the case of methyl groups where their rapid rotation results in Lorentzian decay (Murphy et al., 1982). In the case of the aromatic carbon, where inhomogeneous broadening may lead to overlapping peaks of both protonated and nonprotonated aromatic carbon, the signal decay will record the superposition of both decay trends. This allows for the determination of the fraction of protonated to nonprotonated aromatic carbon. The method has been used extensively and successfully to deconvolute the chemical structure of complex organic solids such as coals (e.g., Hatcher et al., 1989).

In Figure 5, an example of the application of interrupted decoupling is provided using a model compound, 3,5-dimethoxy-4-hydroxy benzoic acid (syngic acid). Only the number 2 and 6 carbons are bonded directly to hydrogen. As seen in Figure 5, their magnetization intensity diminishes rapidly with gaussian decay characteristics. Carbons 3, 4, and 5 are not directly bonded to hydrogen and their magnetization loss exhibits Lorentzian decay characteristics. The methyl carbons follow a more complex decay; although the decay is not, strictly speaking, Lorentzian, the rate of decay is considerably slower than that for carbons 2 and 6, even although they have three times the hydrogen abundance.

Figure 6 presents the interrupted decoupling spectral data for the Murchison organic residue highlighting the loss in magnetization with increasing dephasing time. Spectral intensity in the range of methylene and methine (33 to 45 ppm) carbon is observed to decay rapidly, whereas signal intensity persists for the aromatic resonance (129 ppm and its side bands), as well as for the methyl resonance (at 16 ppm) out to at least 90 μs dephasing time. The resolution of an isolated 16 ppm methyl resonance at long dephasing times supports the assignment of this band to exclusively methyl groups in the previously discussed fast MAS experiments (Figs. 2 and 3; Tables 1 and 2).

The dephasing curves are presented in Figure 7. Both me-

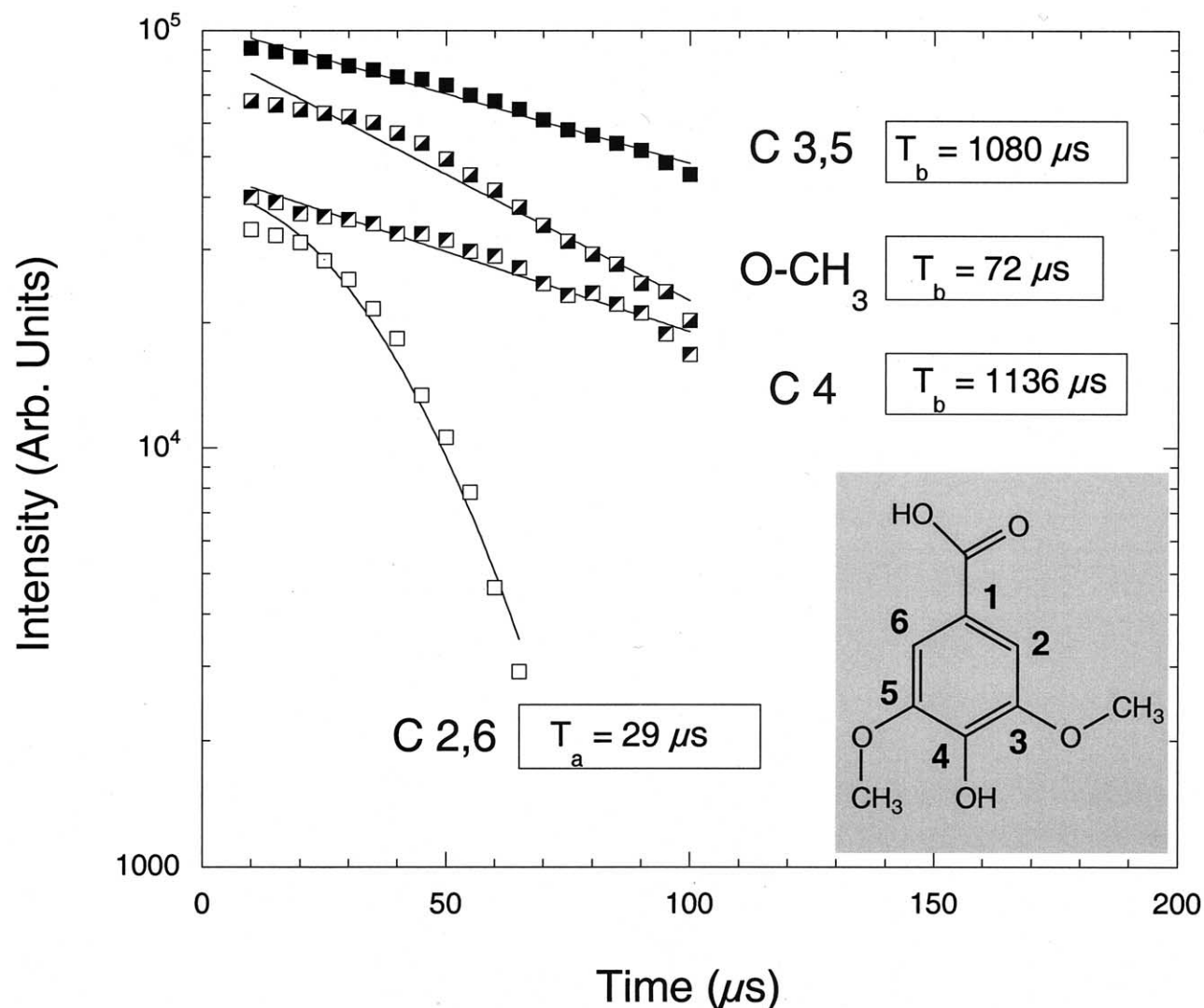


Fig. 5. An example of spectral analysis through interrupted decoupling. With progressive increases in the delay period between the CP contact pulse and the acquisition-proton decoupling stage, signal is lost as a result of dipolar dephasing. These data is for a pure standard (3,5-dimethoxy-4-hydroxy benzoic acid). The curves have been displaced vertically for clarity. The two protonated carbons (carbons 2 and 6) exhibit rapid signal loss with gaussian decay characteristics. Carbons 3, 4, and 5 exhibit slow dephasing times with Lorentzian decay characteristics. Because of rapid molecular rotation, the methyl groups exhibit much slower signal loss resulting from dephasing.

thine (~ 45 ppm) and methylene (~ 32 ppm) exhibit classic gaussian decay behavior, as would be expected, whereas the methyl peak (~ 16 ppm) exhibits Lorentzian decay. The aromatic resonance (~ 130 ppm) exhibits a dual mode for decay, initially gaussian followed by Lorentzian; the fit of this data (Table 3) shows that the fraction of the gaussian component (aromatic carbon bonded to hydrogen) is ~ 0.30 and that the fraction of the Lorentzian component (nonprotonated aromatic carbon) is ~ 0.70 . The uncertainty is estimated to be on the order of ± 0.08 on the basis of the signal to noise.

3.8. Slow-Spinning CP MAS ^{13}C NMR with and without ^1H Decoupling

An alternative to interrupted decoupling experiments involves collecting CP-MAS spectra with and without high

power ^1H decoupling. In the case of pure crystalline solid compounds—for example, syringic acid—acquisition of a CP-MAS spectrum without proton decoupling results in the complete disappearance of signal intensity at the 2 and 6 carbons, as well as that for the methyl carbons. The remaining peaks are broadened substantially. In the case of the Murchison organic residue, the extent of inhomogeneous broadening even with high power proton decoupling is enormous, hence the principal effect of collecting a CP-MAS spectrum without proton decoupling is to quench signal intensity from carbon immediately bonded to carbon without imparting significant broadening.

Figure 8 presents CP-MAS spectra with and without ^1H coupling. The greatest loss in signal intensity occurs in the low-frequency region of the spectrum. Subtracting these two spectra results in Figure 9, where the residual signal corre-

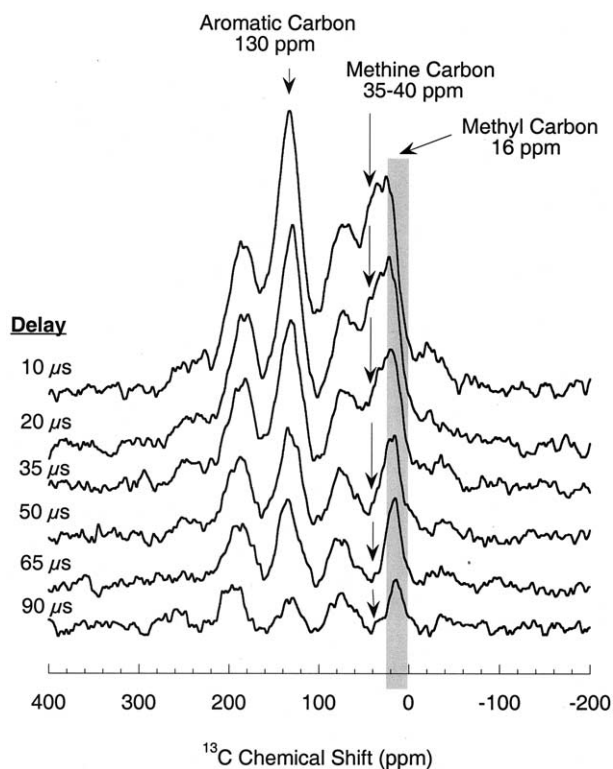


Fig. 6. Stack plot of CP MAS (4 kHz) spectra of the Murchison organic macromolecule with dephasing times ranging from 10 to 90 μs . The spectral region near 35 to 40 ppm exhibits a rapid loss in signal intensity, consistent with resonance intensity in this region being due to the presence of methylene and methine carbon. At around 50 to 65 μs , the only intensity left in the aliphatic region is a single peak at ~ 16 ppm, which is consistent with the presence of methyl carbon. Intensity due to aromatic carbon and its side bands persists out to 90 μs , consistent with a high proportion of aromatic carbon being nonprotonated.

sponds (predominantly) to carbon directly bonded to hydrogen. The difference spectrum corresponds to 31% of the area of the CP-MAS with ^1H decoupling spectrum (Fig. 8) indicating that approximately 31% of the carbon in the Murchison organic residue is protonated. The most intense peak in Figure 9 is centered at 25 ppm and corresponds to undifferentiated aliphatic carbon, the remainder corresponds to predominantly protonated aromatic carbon and its spinning side bands. What is desired is the proportion of intensity shown in Figure 9 that is aromatic and aliphatic, respectively.

Deconvolving Figure 9 into aliphatic and aromatic components is complicated by the overlap of the aromatic carbon's high field spinning side bands with the aliphatic peaks; specifically the side bands at 76 and 22 ppm (the side band at -31 ppm is well separated from the aliphatic region). There are two constraints that facilitate this task. First, the peak shape characteristics of side bands must be identical to that of the central peak. Second, their position is determined precisely by the sample spinning speed. The side band at 76 ppm is confidently fitted by these constraints. The second side band at 22 ppm is fitted by fixing the peak shape characteristics from the isotropic peak at 129 ppm and setting its integrated intensity to lie midway between those of the 76 and -31 ppm peaks. A test of

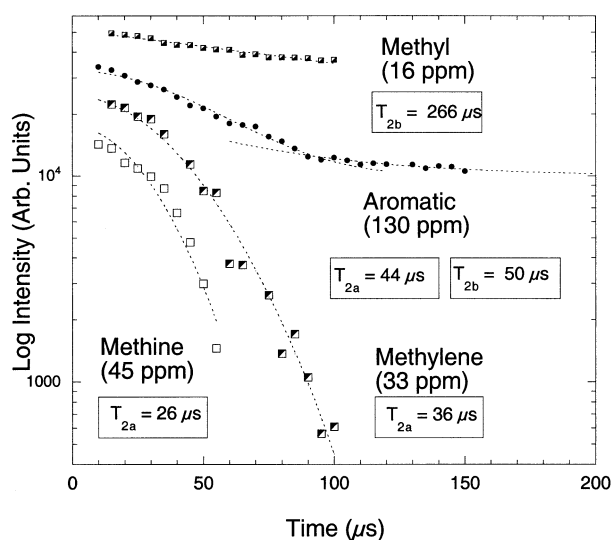


Fig. 7. The loss of signal intensity due to dipolar dephasing for methyl (16 ppm), methylene (32 ppm), methine (45 ppm), and aromatic (130 ppm) carbon. The curves have been displaced vertically for clarity. Intensity at 32 and 45 ppm decays rapidly with gaussian decay characteristics (spin-spin relaxation type *a*, T_{2a}). Methyl carbon signal decays slowly following Lorentzian decay characteristics (spin-spin relaxation type *b*, T_{2b}). Aromatic carbon exhibits an initial gaussian decay followed by Lorentzian decay, behavior consistent with a small amount of protonated aromatic carbon superimposed on a large resonance due to nonprotonated carbon, $\sim 30\%$ (T_{2a}) and 70% (T_{2b}).

this assumption was made by analyzing the low-frequency side band intensities of the protonated aromatic carbon in syringic acid (carbons 2 and 6; Fig. 5). It is observed that the intensity of the third side band is within $\pm 5\%$ of the mean intensity of the second and fourth side bands, supporting this approximation. In general, however, this approach is justified by the well understood systematic behavior of side band intensities (e.g., Herzfeld and Berger, 1980).

The difference spectrum in Figure 9 has $54 \pm 2\%$ of its intensity from aromatic carbon and $46 \pm 2\%$ from aliphatic carbon. By use of these data, we can now estimate (independently of the previous experiments) both the aromaticity and the fraction of protonated aromatic carbon. Note, that also contributing to the nonhydrogen bearing fraction is carboxylate and carbonyl. These values cannot be reliably obtained at slow spinning speeds, consequently we use the values derived from the high-speed CP and SP experiments (Figs. 2 and 3; Tables 1 and 2). Taken together the range in F_a derived from Figures 8 and 9 is from 62.1 to 66.7 (Table 4); this is in reasonable agreement with the analysis of both the high-speed CP and SP spectra (Tables 1 and 2). The fraction of protonated aromatic carbon is ~ 0.30 (Table 4), in reasonable agreement with the interrupted decoupling experiment (Table 3).

3.9. Solid-State ^1H MAS NMR, Constraint on Aliphatic Moieties, and Refinement of NMR-Derived Hydrogen Content

Solid-state ^1H -NMR is complicated by strong dipolar coupling between protons. The strength of this coupling (on the order of 50 kHz) leads to extreme homogeneous line broaden-

Table 3. Dynamic parameters derived from variable contact time and interrupted decoupling solid-state CP NMR experiments (MAS frequency = 4 kHz)

Peak (ppm)	T_{CH} (μ s)	$T_{1\rho}$ (ms)	T_{2a} (μ s)	T_{2b} (μ s)	I_a^a	I_b^b
16 (methyl)	—	—	—	266	0	100
33 (methylene)	158	7.2	36	—	100	0
45 (methine)	—	—	26	—	100	0
130 (aromatic)	576	9.9	44	50	30 ^c	70

^a Intensity of Gaussian component.

^b Intensity of Lorentzian component.

^c The fraction of protonated aromatic carbon (F_a^H) = 0.30 ± 0.08 .

ing. This effect combined with the narrow chemical shift range of 1H generally leads to totally featureless spectra. There are two means to circumvent this effect. One method exploits the classic Combined Rotation and MultiPulse Spectroscopy (CRAMPS) (e.g., Mehring, 1976). A second method uses extremely fast MAS. In the present study, the latter approach is used. By spinning the sample at 30 kHz, much of the dipolar coupling is averaged to zero. This is demonstrated in Figure 10, where the proton spectrum of the Murchison organic residue reveals an intense central peak surrounded by spinning side bands. The intensity of the side bands reflects the residual strength of the dipolar coupling, which as can be seen in Figure 10 is low.

Expanding the central region (Fig. 11), two peaks are observed; a high-frequency peak (~ 7 ppm) corresponding to aromatic hydrogen and a lower frequency peak (~ 2 ppm) corresponding to aliphatic hydrogen. Even with extremely fast spinning, the 1H spectrum still remains broad. Much of this residual broadening results from disorder in the macromolecular structure such that a given proton's intrinsic frequency is perturbed by proximity to shielding and deshielding fields of

neighboring aromatic rings. Note, however, that the extent of broadening is not in excess of what is observed with CRAMPS when applied to similarly aromatic disordered organic solids, such as coals (e.g., Jurkiewicz et al., 1993).

The spectrum in Figure 11 is fitted with two absorption bands resulting in the fraction of aromatic 1H and aliphatic 1H being 0.30 ± 0.03 and 0.70 ± 0.03 . This is a valuable piece of information, for when combined with the previously determined fractions of protonated aromatic and aliphatic carbon (Table 4), one can use these fractions to establish the distribution of aliphatic functionality in terms of methyl, methylene, and methine. The average hydrogen content of aliphatic carbon, z (as in CH_z), is determined from the combined 1H -NMR data and data from Table 4 by using the relation

$$Z = (F_H^{AL}/F_H^{AR}) \times (F_{CH}^{AR}/F_{CH}^{AL}) \quad (2)$$

where $F_H^{AL,AR}$ are the fractions of aliphatic and aromatic hydrogen, respectively, and $F_{CH}^{AR,AL}$ are the fractions of protonated aromatic and aliphatic carbon, respectively. On the basis of the uncertainty of the fit of the 1H -NMR spectrum (Fig. 11), the

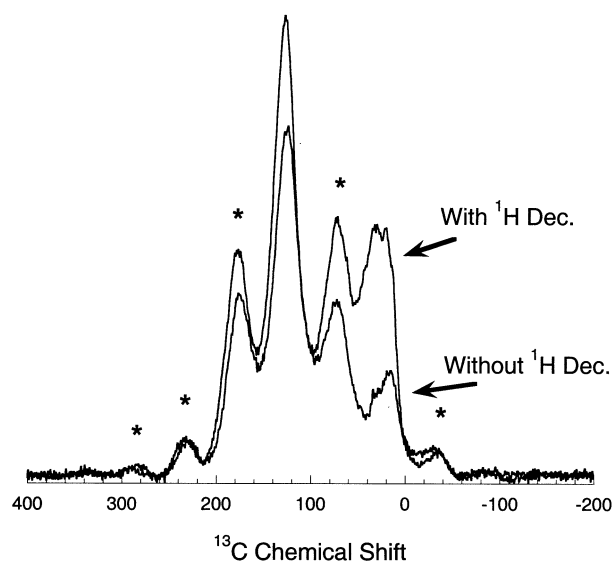


Fig. 8. CP-MAS spectra of the Murchison organic macromolecule with and without high power 1H decoupling. The loss in signal intensity is predominantly in the aliphatic (low frequency) region, although there is some loss exhibited in the aromatic region. Signal loss is due to dephasing of carbon magnetization when carbon is directly bonded to hydrogen.

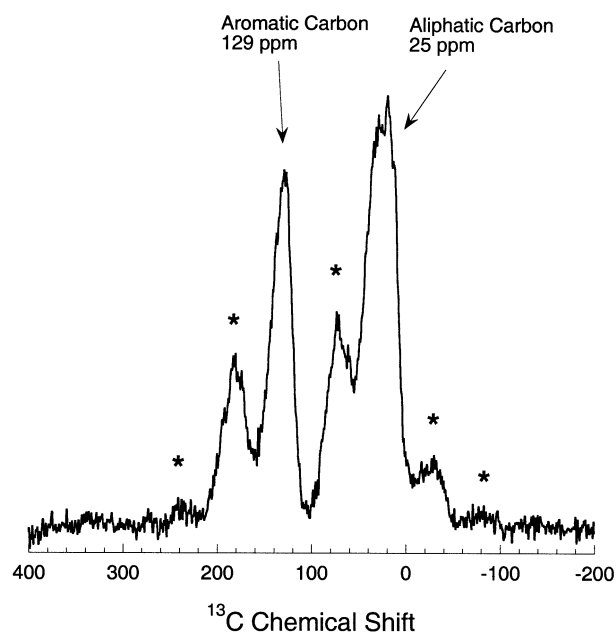


Fig. 9. A difference spectrum derived from subtraction of CP-MAS with and without proton decoupling. The result records the spectrum of carbon directly bonded to hydrogen. Spinning side bands are labeled with an asterisk.

Table 4. Functional group distribution derived from slow-spinning (4 kHz) CP-MAS experiments (with and without ^1H decoupling).

Carbon type	Fraction of carbon	Functional groups	Contribution (%)	Aromatic carbon type (%)
Protonated Carbon	0.36	Al-H	16.6	
Nonprotonated Carbon	0.64	Ar-H	19.4	29–30
		Ar-C,O	45.2–47.5	70–71
		COOH, R	6.8–7.4*	
		R-CO-R'	9.1–12.0*	
			$F_a = 0.65 - 0.67$	

*Values for COOH,R and R-CO-R' are obtained from the fast-spinning (12 kHz) data for both cross-polarization (VACP) and single pulse.

ratios of aromatic to aliphatic hydrogen range from 33:67 (mean, 30:70) to 27:73. The values of z range between 1.8 (H poor), 2.1 (H intermediate), and 2.4 (H rich). Of course z is related to the fractional abundance of methyl, methylene, and methine hydrogen (designated, respectively, as J , K , L , where $J + K + L = 1.0$), as in Eqn. 3:

$$Z = J \times (\text{CH}_3) + K \times (\text{CH}_2) + L \times (\text{CH}). \quad (3)$$

Eqn. 3 is underdetermined. However, from the interrupted decoupling experiment (Fig. 6), it was observed that the methyl groups are constrained to resonate at a frequency of 16 ppm. We therefore constrain Eqn. 3 by fixing the methyl percentage to that derived from 12 kHz ^{13}C solid-state NMR data (Tables 1 and 2) and solve for the methylene and methine content. The sum of methylene and methine include the oxygen-substituted aliphatic carbon (Tables 1 and 2) as the solid NMR spectrum is too broad to differentiate between the aliphatic functional groups.

The results are presented in Table 5, where the analysis of the data incorporates both the CP and SP derived values for the methyl contribution, as well as aromatic hydrogen. The constraint of a fixed proportion of methyl groups acts as a lever,

enhancing the effect of choosing low, medium, or high values of z . Thus, the proportions of methyl, methylene, and methine shift dramatically across the allowed range of z . To calculate the bulk hydrogen content, we chose the case where the oxygen-containing functionality is fully cross-linked, yielding a minimum bulk oxygen content (as described in Tables 1 and 2) consistent with the elemental analyses. The result of these calculations is that the bulk hydrogen content (given as H/C) is 0.65 ± 0.07 for the CP data, but if we include the $\sim 3\%$ interstellar diamond, the bulk H/C would drop to 0.63 ± 0.07 . For the SP data the bulk H/C is 0.58 ± 0.06 , or 0.53 ± 0.06 when the SP data from Table 2 is corrected for the presence of $\sim 3\%$ interstellar diamond.

4. CONCLUSIONS

The application of independent yet complementary solid-state ^1H and ^{13}C -NMR experiments yields a robust and self-consistent picture of the organic chemistry of the Murchison organic macromolecule. The data derived from this study lead to the following conclusions.

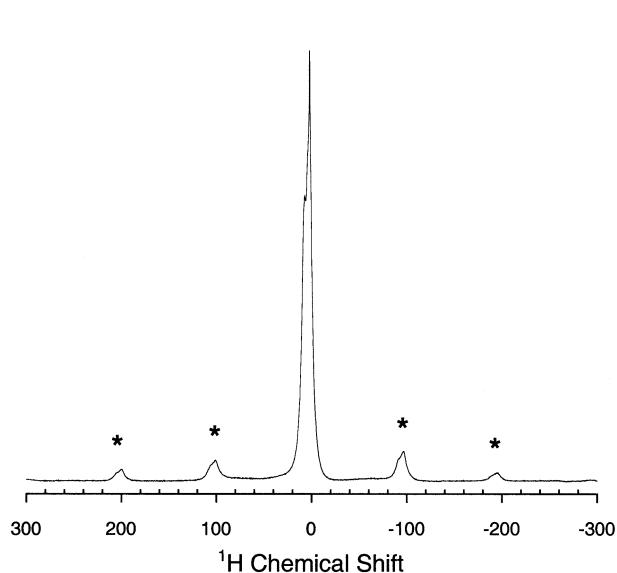


Fig. 10. High-speed MAS (30 kHz) SP ^1H -NMR spectrum of the Murchison organic macromolecule using the DEPTH pulse sequence for background suppression. The intensity of the spinning side bands (indicated by an asterisk) reflect the magnitude of the residual dipolar coupling.

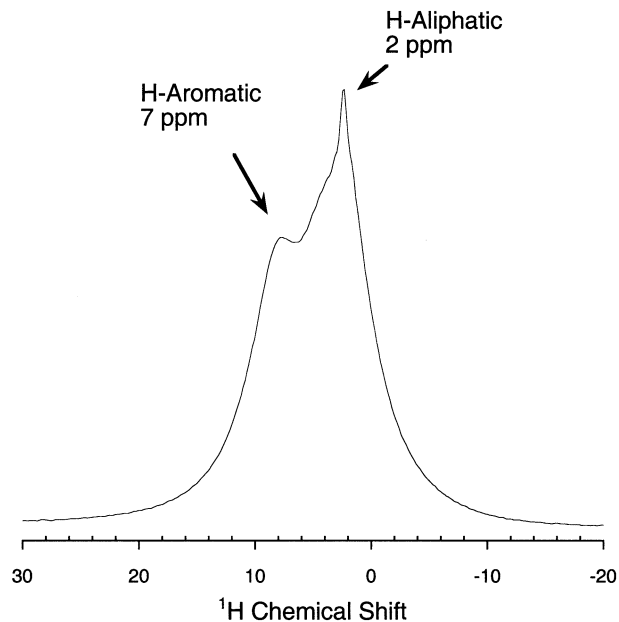


Fig. 11. Expanded region of the SP MAS ^1H -NMR spectrum showing the "fine" structure—that is, broad resonances for aromatic protons at (~ 7 ppm) and aliphatic protons at (~ 2 ppm).

Table 5. Estimated aliphatic carbon distributions and bulk hydrogen content derived from ^1H and ^{13}C solid-state NMR data.

$H_{\text{AR}}:H_{\text{AH}}$	Cross-polarization data						Single-pulse data					
	33:67		30:70		27:73		33:67		30:70		27:73	
	%C ^a	%H	%C ^a	%H	%C ^b	%H	%C ^c	%H	%C ^c	%H	%C ^a	%H
CH_3	8.0	24.0	8.0	24.0	8.6	25.8	7.3 (6.4) ^d	21.9 (19.2)	9.7 (8.6)	29.1 (25.8)	9.7 (10.0)	29.1 (30.0)
CH_2	1.5	3.0	7.6	15.2	13.5	27.0	0.0 (0.0)	0.0 (0.0)	0.4 (0.0)	0.8 (0.0)	6.5 (2.8)	13.0 (5.6)
CH	12.7	12.7	6.7	6.7	0.0	0.0	11.3 (9.8)	11.3 (9.8)	8.5 (7.6)	8.5 (7.6)	2.4 (3.4)	2.4 (3.4)
$\text{C}_{\text{AR}}\text{-H}$	18.4		18.4		18.4		18.7 (19.3)		18.7 (19.3)		18.7 (19.3)	
H/C^{e}	0.58		0.64		0.71		0.50 (0.48)		0.57 (0.53)		0.63 (0.58)	

^a Calculations fix the methyl content to that derived from 12 kHz CP and SP ^{13}C solid-state NMR.

^b Methyl content relaxed as aliphatic hydrogen content is too high for 8.0% methyl plus remaining aliphatic functionality.

^c Methyl content relaxed as aliphatic hydrogen content is too low for 9.7% methyl plus remaining aliphatic functionality.

^d Values in parentheses are corrected to account for $\approx 3\%$ intensity in the SP spectrum derived from interstellar diamond.

^e Adopts the case of maximum linking among oxygen functionality; therefore, the only sources of H are from aliphatic and aromatic moieties.

(1) The F_a within the Murchison organic residue is now considerably better constrained and lies between 0.61 and 0.66, as determined by three independent measurements. The maximum and minimum values are derived from independent CP ^{13}C -NMR measurements, whereas estimates derived from SP ^{13}C -NMR lie closer to the higher value.

(2) The CP and SP ^{13}C -NMR spectra reveal a similar distribution of carbon functionality. Such similarity requires that quantities of large so-called laterally condensed molecules on the scale of coronene, ovalene, or larger are not significant. The difference in F_a between the 12-kHz MAS CP and SP ^{13}C -NMR data could accommodate up to 10% of these larger, hydrogen-poor molecules. The NMR data do not place constraint on the size of cata-condensed polycyclic aromatic compounds such as phenanthrene, chrysene, and larger, because carbon in these compounds will be readily detected by using CP methods.

(3) The previously derived conclusion that CP methods (Cronin et al., 1987; Gardinier et al., 2000) do not detect significant quantities of nonprotonated aromatic carbon in the macromolecule—for example, 19 to 33% and up to 40%—based on F_a derived by Cronin et al. (1987) is invalidated. The previously published CP ^{13}C -NMR experiments overrepresented the abundance of aliphatic carbon due to their choice of CP contact time.

(4) The F_a that is directly bonded to hydrogen is low ($\sim 30\%$). Because the close similarity between the 12-kHz CP and SP MAS data preclude the presence of large quantities of large laterally condensed aromatic molecules, this indicates that aromatic molecules in the Murchison organic residue are highly substituted. This is a critical parameter to consider when formulating a statistical molecular picture of the Murchison organic macromolecule. This conclusion is also consistent with previous statements made by Sephton et al. (1999), who concluded that earlier studies had overestimated the concentration of large laterally condensed organic molecules as a result of analytical schemes that lead to a loss of smaller, more volatile, aromatic molecules.

(5) The hydrogen content, as derived from NMR data, lies in the range of estimates that exist in the literature, provided that there exists a high degree of cross-linking among oxygen-containing organic functionality. The quantity of oxygen-containing organic functionality in the Murchison macromolecule

is significant. Depending on whether various oxygen-containing organic functional groups exist as free acids and hydroxyl dictates a huge range in O/C. It appears reasonable to favor the lowest O/C estimates as they are closer to estimates derived from elemental analysis. Furthermore, the lower O/C values yield more reasonable values for H/C.

(6) A significant proportion of tertiary (methine, CH) carbon is indicated by the combined analysis of the ^1H and ^{13}C solid-state NMR data. This reveals that aliphatic carbon chains within the Murchison organic macromolecule are highly branched.

The picture of the chemical structure of the Murchison organic residue that emerges from this analysis is one of a structurally complex, extensively cross-linked, and highly aromatic macromolecule. It should be noted that molecular data derived from degradative analysis of the Murchison reveal a broad range of aromatic and aliphatic molecular constituents (e.g., Hayatsu and Anders, 1981; Sephton et al., 2000); the NMR data average across this complexity. The NMR and elemental data discussed in this article serve to provide compositional boundary conditions for any molecular structural model that may be proposed for the insoluble organic residue in the Murchison. Before this step, however, more information must be obtained regarding the types and abundance of the oxygen-, nitrogen-, and sulfur-containing organic functional groups. Such studies are in progress. Once a molecular structural model of the Murchison organic macromolecule is derived that is both consistent with these NMR data and including the range in molecular species identified via degradative techniques, we can begin to consider a viable pathway back from this enigmatic material to its solar or interstellar origins.

Acknowledgments—The authors gratefully acknowledge the financial support through a grant from NASA's Origins of the Solar System Program (NASA-NC00-227). We also thank Dr. Glenn MacPherson (Smithsonian Institution) for generously providing the sample of the Murchison meteorite. The elemental analysis and direct determination of oxygen content was kindly performed by Dr. Marilyn Fogel (GL). Dr. Hugh Hill (NASA-Goddard) kindly loaned us the sample of the 4-nm detonation diamond. We extend our thanks to Dr. Mark Sephton and two anonymous reviewers for their careful and helpful reviews. We also thank Drs. Larry Nittler (DTM), John Muntean (ANL), and Wes Huntress (GL) for helpful comments on an early version of this manuscript. All NMR analyses were performed at the W. M. Keck solid-state NMR facility at the Geophysical Laboratory, Carnegie Institution of

Washington, funded through the generous support of the National Science Foundation (EAR-MRI 9724317), the W. M. Keck Foundation, and the Carnegie Institution of Washington.

Associate editor: C. Koeberl

REFERENCES

- Alemayehu L. B., Grant D. M., Alger T. D., and Pugmire R. J. (1983) Cross polarization and magic angle sample spinning NMR spectra of model organic compounds III. The effect of ^{13}C - ^1H interaction on cross polarization and carbon-proton dephasing. *J. Am. Chem. Soc.* **105**, 6697–6704.
- Alexander C. M. O'D., Russell S. S., Arden J. W., Ash R. D., Grady M. M., and Pillinger C. T. (1998) The origin of chondritic macromolecular organic matter: A carbon and nitrogen isotope study. *Meteor. Planet. Sci.* **33**, 603–622.
- Cody G. D., Alexander C. M. O'D., and Tera F. (1999) New insights into the chemistry of the Murchison organic macromolecule using high field ^{13}C solid state NMR. *Lunar Planet. Sci.* **30**, CD 1582.
- Cronin J. R., Pizzarello S., and Frye J. S. (1987) ^{13}C NMR spectroscopy of insoluble carbon of carbonaceous chondrites. *Geochim. Cosmochim. Acta* **51**, 299–303.
- Cronin J. R., Pizzarello S., and Cruickshank D. P. (1988) Organic matter in carbonaceous chondrites, planetary satellites, asteroids, and comets. In *Meteorites and the Early Solar System* (eds. J. F. Kerridge and M. S. Mathews), pp. 819–857. University of Arizona Press.
- Desch S. J. and Cuzzi J. N. (2000) The generation of lightning in the Solar Nebula. *Icarus* **143**, 87–105.
- Ernst R. H., Bodenhausen G., and Wokaun A. (1991) *Principles of Nuclear Magnetic Resonance in One and Two Dimensions*. Clarendon Press.
- Gardinier A., Derenne S., Robert F., Behar F., Largeau C., and Maquet J. (2000) Solid state CP/MAS ^{13}C NMR of the insoluble organic matter of the Orgueil and Murchison meteorites: Quantitative study. *Earth Planet. Sci. Lett.* **184**, 9–21.
- Hartmann S. R. and Hahn E. L. (1962) Nuclear double resonance in the rotating frame. *Physical Rev.* **128**, 2042–2053.
- Hatcher P. G., Lerch H. E., Bates A. L., and Verheyen T. V. (1989) Solid state ^{13}C nuclear magnetic resonance studies of coalified gymnosperm xylem tissue from Australian brown coals. *Org. Geochem.* **14**, 145–155.
- Hayatsu R., Matsuoka S., Scott R. G., Studier M. H. and Anders E. (1977) Origin of organic matter in the early solar system—VII: The organic polymer in carbonaceous chondrites. *Geochim. Cosmochim. Acta* **41**, 1325–1339.
- Hayatsu R., Winans R. E., Scott R. G., McBeth R. L., Moore L. P., and Studier M. H. (1980) Phenolic ethers in the organic polymer of the Murchison meteorite. *Science* **207**, 1202–1204.
- Hayatsu R. and Anders E. (1981) Organic compounds in meteorites and their origins. In *Topics of Current Chemistry*, pp. 1–37. Springer-Verlag.
- Herzfeld J. and Berger A. E. (1980) Sideband intensities in NMR spectra of samples spinning at the magic angle. *J. Chem. Phys.* **73**, 6021–6030.
- Jurkiewicz A., Bronnimann C. E., and Maciel G. E. (1993) High resolution ^1H NMR studies of Argonne premium coals. In *Magnetic Resonance of Carbonaceous Solids* (eds. R. E. Botto and Y. Sanada), pp. 401–419. Advances in Chemistry Series 229. American Chemical Society.
- Kerridge J. F. (1983) Isotopic composition of carbonaceous chondrite kerogen: Evidence for an interstellar origin of organic matter in meteorites. *Earth Planet. Sci. Lett.* **64**, 186–200.
- Kerridge J. F. (1985) Carbon, hydrogen, and nitrogen in carbonaceous chondrites: abundances and isotopic compositions in bulk samples. *Geochim. Cosmochim. Acta* **49**, 1707–1714.
- Kerridge J. F., Chang S., and Shipp R. (1987) Isotopic characterization of kerogen-like material in the Murchison carbonaceous chondrite. *Geochim. Cosmochim. Acta* **51**, 2527–2540.
- Kress M. E. and Tielens S. (2001) The role of Fischer-Tropsch catalysis in solar-nebula chemistry. *Meteor. Planet. Sci.* **36**, 75–82.
- Kress M. E., Desch S. J., Dateo C. E., and Benedix G. (2001) Shock processing of interstellar nitrogen: Compounds in the Solar Nebula. *Adv. Space Res.*, in press.
- Lewis R. S., Ming T., Wacker J. F., Anders E. and Steel E. (1987) Interstellar diamonds in meteorites. *Nature* **326**, 160–162.
- Mehring M. (1976) *High Resolution NMR Spectroscopy in Solids*. Springer-Verlag.
- Miller S. L. (1955) Production of some organic compounds under possible primitive Earth conditions. *J. Am. Chem. Soc.* **77**, 2351–2362.
- Morgan W. A., Jr., Feigelson E. D., Wang H., and Frenklach M. (1991) A new mechanism for the formation of meteoritic kerogen-like material. *Science* **254**, 109–111.
- Murphy P. D., Cassady T. J., and Gernstein B. C. (1982) Interrupted decoupling ^{13}C solid state NMR of coals. *Fuel* **61**, 1233–1240.
- Pines A., Gibby M. G., and Waugh J. S. (1973) Proton-enhanced NMR of dilute spins in solids. *J. Chem. Physics* **39**, 569–590.
- Robert F. and Epstein S. (1982) The concentration and isotopic composition of hydrogen, carbon, and nitrogen in carbonaceous meteorites. *Geochim. Cosmochim. Acta* **46**, 81–95.
- Sagan C. and Khare B. N. (1979) Tholins: Organic chemistry of interstellar grains and gas. *Nature* **277**, 102–105.
- Septon M. A., Pillinger C. T., and Gilmour I. (1999) Small-scale hydrous pyrolysis of macromolecular material in meteorites. *Planet. Space Sci.* **47**, 181–187.
- Septon M. A., Pillinger C. T., and Gilmour I. (2000) Aromatic moieties in meteoritic macromolecular materials: Analysis by hydrous pyrolysis and $\delta^{13}\text{C}$ of individual compounds. *Geochim. Cosmochim. Acta* **64**, 321–328.
- Snape C. E., Ladner W. R., and Bartle K. D. (1979) Survey of carbon-13 chemical shifts in aromatic hydrocarbons and its application to coal-derived materials. *Anal. Chem.* **51**, 2189–2197.
- Tsiao C. and Botto R. E. (1993) Measurement of spin-lattice relaxation in Argonne premium coal samples. In *Magnetic Resonance of Carbonaceous Solids* (eds. R. E. Botto and Y. Sanada), pp. 341–358. Advances in Chemistry Series 229. American Chemical Society.
- van Krevelan D. W. (1993) *Coal*. Elsevier.
- Werhli F. W. and Wirthin T. (1976) *Interpretation of Carbon-13 Spectra*. Hayden.
- Wind R. A., Maciel G. E., and Botto R. E. (1993) Quantitation in ^{13}C NMR spectroscopy of carbonaceous solids. In *Magnetic Resonance of Carbonaceous Solids* (eds. R. E. Botto and Y. Sanada), pp. 3–26. Advances in Chemistry Series 229. American Chemical Society.
- Yang J. and Epstein S. (1983) Interstellar organic matter in Murchison meteorite. *Geochim. Cosmochim. Acta* **47**, 2199–2216.
- Yang J. and Epstein S. (1984) Relic interstellar grains in Murchison meteorite. *Nature* **311**, 544–547.
- Zinner E. (1988) Interstellar cloud material in meteorites. In *Meteorites and the Early Solar System* (eds. J. F. Kerridge and M. S. Mathews), pp. 956–983. University of Arizona Press.